# Mott–Schottky Analysis of the P3HT:$ZnS_{cubic}$ and P3HT:$ZnS_{hexa}$ Bulk Heterojunction Solar Cells

T. Abdul Kareem*

Radiation Physics at the Department of Physics, University of Calicut, 673635 Kerala, India

*(Received December 6, 2015; in final form February 8, 2016)*

Bulk heterojunction solar cells of sphalerite and wurtzite ZnS incorporated P3HT were fabricated and their Mott–Schottky analysis was performed to find the conduction mechanism of the devices. The analysis shows the formation of a Schottky junction and band unpinning at the P3HT:ZnS-Al contact and it confirms the hole conductivity in the active material.

DOI: 10.12693/APhysPolA.129.409

PACS/topics: 87.85.Rs, 73.40.Lq, 73.40.Sx, 73.50.Pz, 73.61.Ga, 73.61.Ph, 73.63.Bd, 81.05.Dz, 88.40.jp, 88.40.jr

## 1. Introduction

Bulk heterojunction solar cells made of conducting polymers represent a new stage in the evolution of photovoltaic devices and this type of excitonic cells are presently the most studied solar cells [1–5]. In the case of "bulk heterojunction", the interface between two materials of different electrical properties is all over the bulk, where the electron accepting nanoparticles are mixed with the electron donating polymer and the exciton created in either material diffuse to the interface to enable the charge separation. Poly(3-hexyl) thiophene (or P3HT):ZnS are very interesting nanocomposites due to their applicability as an active layer for bulk heterojunction solar cells of high open circuit voltage [6–8] and the charge transport in this system determines the performance of solar cells made of this nanocomposites. This paper discusses the Mott–Schottky characteristics of solar cells made of inorganic semiconducting ZnS nanoparticles with organic P3HT. Here, ZnS nanoparticles are preferred as an electron acceptor because it is environment friendly, stable indefinitely, and can be synthesized easily and inexpensively. It is supposed here that the lowest unoccupied molecular orbital (LUMO) level of the ZnS is below at least 0.3 eV than that of P3HT for an effective exciton splitting and charge dissociation [9], since quantum confinement effect of the semiconducting nanocrystals shifts their LUMO level to upward and the highest occupied molecular orbital (HOMO) to downward and that enlarges the band gap [10]. The wide band semiconductor ZnS has high electron mobility (600 $cm^2\ V^{-1}\ s^{-1}$ [11]) and has an electron affinity of about 3.9 eV [12] that makes ZnS as an attractive material to use as an electron acceptor in hybrid photovoltaic devices. Further, conduction band shifts upward as decreasing the size of the particle [10] that helps to match well with the LUMO level of P3HT, therefore ZnS nanoparticles provide the right morphology for the acceptance of electron.

*corresponding author; e-mail: abdulkareem.t@gmail.com

## 2. Materials and methods

Performance of bulk heterojunction solar cells strongly depends on the processing conditions such as film thickness, donor/acceptor mixing ratio, and thermal annealing time and temperature. Therefore, the devices for this study were fabricated by considering the previously reported optimized condition of the standard P3HT/PCBM and P3HT/ZnS devices [7]. All chemicals such as PEDOT:PSS, P3HT and indium tin oxide glass slides (surface resistivity is about 8 to 12 $\Omega/m^2$ and having thickness about 1200 Å) were purchased from Sigma Aldrich Chemicals Ltd., Bangalore. Sphalerite and wurtzite ZnS nanoparticles [13, 14] of better performance for the solar cells were prepared in our lab by simple wet chemical method. Here the active layer of the solar cell was sandwiched in between ITO (work function ≈4.8 eV [15]) and aluminium (work function ≈4.1 eV [16]) to generate a built-in electric field by the difference in their work functions. This built-in electric field is used to dissociate the excitons generated by the absorption of light in the active layer, where the transparent ITO layer is used as a top electrode facing the sun light. It is a well-known fact that thin film of ITO has low electrical resistivity ($\approx 5 \times 10^{-4}\ \Omega$ cm [17]) and has band gap of about 3.8 eV [18]. Furthermore, ITO is a good hole injector [19] and therefore it can be used as anode. In principle, ITO is capable of collecting either electrons or holes since its work function (*ca.* 4.2–5.3 eV) lies between the typical HOMO and LUMO of common organic photovoltaic (OPV) materials. Accordingly, the polarity of ITO can be modified to efficiently collect either electrons or holes by coating with functional interlayers of different work functions such as PEDOT:PSS [20], so that 50 nm thick PEDOT:PSS film were coated over the ITO by making a solution of PEDOT:PSS (2 ml) with surfactant Triton-100 (50 $\mu$l). Then one drop of the filtered (by a 0.45 $\mu$m nylon filter) PEDOT:PSS solution applied over the ITO and coated a 50 nm thick film using a spinner at 3000 rpm for 10 s.

TABLE I

Thickness of the active layer.

| Sample name | Thickness [nm] |
|---|---|
| Glass/P3HT:$ZnS_{cubic}$ | 247 |
| Glass/P3HT:$ZnS_{hexa}$ | 275 |

Active layer ZnS:P3HT solution were made by mixing P3HT in 20 mg/ml in dichlorobenzene with the synthesized (1) 1 mg of $ZnS_{cubic}$ nano particles and (2) 1 mg of $ZnS_{hexa}$ nano particles. All the samples were kept under stirring for 24 h, then each drop of the samples was placed over the previously prepared ITO:PEDOT:PSS films and over cleaned plane glass slides also, where the spinner spinned at 3000 rpm for 10 s in each case, where one edge of the plane glass slides was covered with cellophane tape to make "step" for thickness measurement and the thickness of the active layer found as given in Table I using a noncontact 3D Profiler (Taylor Hobson Talysurf CCI MP interferometer).

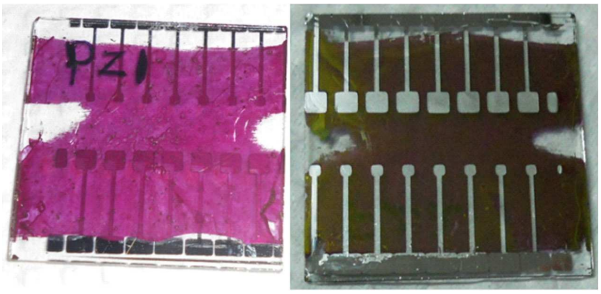


Fig. 1. Solar cell of structure ITO/PEDOT:PSS/P3HT:$ZnS_{cubic}$/Al.

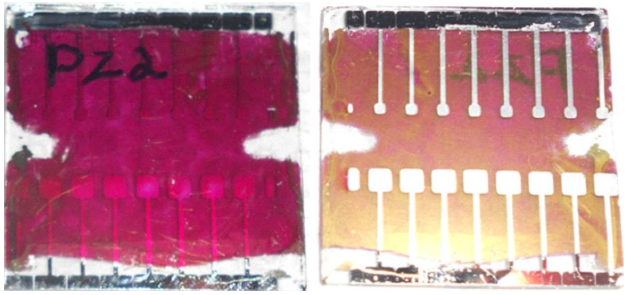


Fig. 2. Solar cell of structure ITO/PEDOT:PSS/P3HT:$ZnS_{hexa}$/Al.

A chromium mask with device areas $1 \times 10^{-6}$ m$^2$ (1 mm × 1 mm) and $4 \times 10^{-6}$ m$^2$ (2 mm × 2 mm) was placed over the active layer and kept the samples in the thermal evaporator 10 inch away from the molybdenum boat containing 81 mg of Al pellets. Pressure inside the chamber was maintained as $5 \times 10^{-5}$ mbar and applied a voltage of 3 V and 25 A current for coating the Al. Thickness was monitored using the crystal thickness monitor and the coating process was stopped when the thickness was about 105 nm. Final devices are shown in Fig. 1 and Fig. 2, where the small devices have area about $1 \times 10^{-6}$ m$^2$ and the bigger is about $4 \times 10^{-6}$ m$^2$. Two probe $I$–$V$ measurements of the prepared solar cells were noted by Oriel Sol3A Solar Simulator under illuminated and non-illuminated conditions and the results are given in Table II and Table III.

TABLE II

ITO/PEDOT:PSS/P3HT:$ZnS_{cubic}$/Al device — solar cell parameters.

| Mode | $P_{max}$ [nW] | $I_{pm}$ [nA] | $V_{pm}$ [V] | $J_{sc}$ [$\mu$A/cm$^2$] | $V_{oc}$ [V] | FF | $E_{ff}$ [%] | $R_s$ [MΩ] | $R_{sh}$ [MΩ] |
|---|---|---|---|---|---|---|---|---|---|
| light | 146.441 | 430.708 | 0.340 | 30.100 | 1.120 | 0.109 | 0.0037 | 4.120 | 0.261 |
| dark | 1.131 | 2.759 | 0.410 | 0.716 | 0.820 | 0.193 | 0.0001 | 5.137 | 64.014 |

TABLE III

ITO/PEDOT:PSS/P3HT:$ZnS_{hexa}$/Al device — solar cell parameters.

| Mode | $P_{max}$ [nW] | $I_{pm}$ [nA] | $V_{pm}$ [V] | $J_{sc}$ [$\mu$A/cm$^2$] | $V_{oc}$ [V] | FF | $E_{ff}$ [%] | $R_s$ [MΩ] | $R_{sh}$ [MΩ] |
|---|---|---|---|---|---|---|---|---|---|
| light | 323.317 | 769.802 | 0.420 | 229.60 | 1.300 | 0.108 | 0.0320 | 1.765 | 0.124 |
| dark | 8.293 | 17.277 | 0.480 | 3.74 | 0.959 | 0.231 | 0.0008 | 22.261 | 17.846 |

## 3. Results and discussion

UV-Vis measurements of the active layer P3HT:ZnS obtained by Varian, Cary 5000 Spectrophotometer is given in Fig. 3 and it shows a broad absorption from 400 nm to 650 nm. Previous reports of P3HT shows broad absorption spectra from 320 to 650 nm and it varied depending on the solvent but around 500 nm, that can be attributed to the $\pi$–$\pi^*$ transitions [8]. The obtained UV–Vis spectrum is simply the combination of constituents parts of the active materials i.e. nanocrystals and polymer and it is seen that there is no any additional absorption peaks [8] since there is not any ground state interactions between them [21]. It is seen that the absorption edge of the ZnS:P3HT little extended to the lower wavelength region and that may be due to the quantum confinement effect from the inorganic nano particles [8]. This blue shift may be due to the rising in band gap between $\pi$ and $\pi^*$ energy levels when adding the nanoparticles that decreases the inter-chain interaction and conjugation length of P3HT [8].

It is a well-known fact that P3HT is a conjugated polymer that easily undergoes $p$-doping (reacting with oxygen) when exposed to air or moisture, consequently the Schottky contacts are formed at the semiconductor–metal interface, so that the effect of band bending (depletion zones) and minority carrier injection should be considered [22]. Therefore the Mott–Schottky analysis were performed on the devices ITO/PEDOT:PSS/P3HT:$ZnS_{cubic}$/Al and ITO/PEDOT:PSS/P3HT:$ZnS_{hexa}$/Al that can reveal the fundamental parameters in heterojunctions such as charge carrier concentrations and the inbuilt potential. The Mott–Schottky information will be obtained from

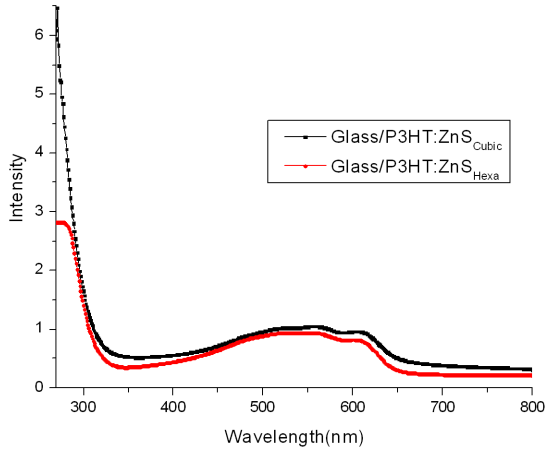


Fig. 3. UV-Visible absorption spectrograph of the active layer.

the capacitance–voltage measurements and here dc Probe Station 2 (PM5, Agilent Device Analyzer B1500A with pulsed source 5 MHz) at the CeN Facility, IISc, Bangalore was used for these measurements.

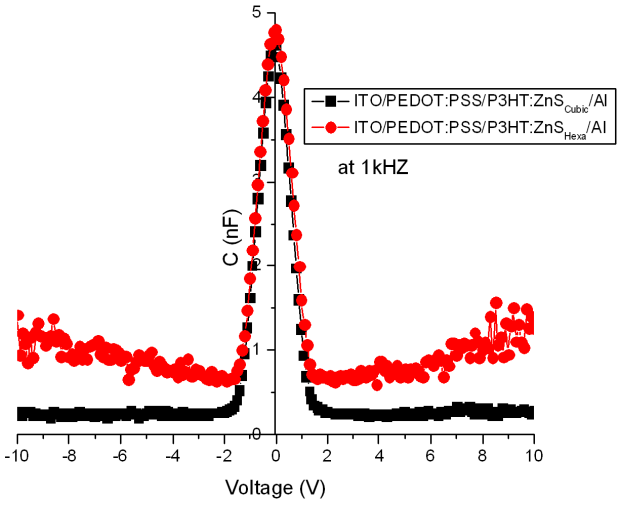


Fig. 4. Capacitance–voltage characteristics of the devices.

The procedure for taking $C$–$V$ measurements involves the application of dc bias voltages across the capacitor (polymer solar cells) by connecting the Al side to earth terminal while making the measurements with an ac signal with frequency of 1 kHz after discussion with supervisory team, since higher frequencies will have a negative impact on the devices. This change in potential increases the space of the charge and therefore the capacitance. This differential capacitance can be measured at different dc potentials in order to obtain the capacitance–voltage characteristic. The bias applied as a dc voltage sweep that drives the device structure from its accumulation region into the depletion region, and then into inversion region. Figure 4 shows the direct measurement of the capacitance under reverse and forward voltages of the bulk heterojunction structure of the two devices ITO/PEDOT:PSS/P3HT:ZnS$_{\text{cubic}}$/Al and ITO/PEDOT:PSS/P3HT:ZnS$_{\text{hexa}}$/Al.

Figure 4 shows that the charge carriers accumulate near the interface at zero voltage so that the capacitance is maximal (i.e., $d$ is minimal). According to the bias voltage, carriers get pushed away from the oxide interface and the depletion region forms. When the bias voltage is reversed, the charge carriers move the greatest distance from the interface so that the capacitance decreases and becomes minimum at maximum $d$ according to the equation

$$\varepsilon = \frac{C_d}{\varepsilon_0 A} \tag{3.1}$$

and the depletion width can be found from the equation

$$W = \sqrt{\frac{2\varepsilon\varepsilon_0(V_{\text{bi}} + V)}{qN}}. \tag{3.2}$$

One side of the heterojunction has a charge density higher than the other and therefore the capacitance voltage characteristics can be approximated by [23]:

$$\frac{A^2}{C^2} = \frac{2}{q\varepsilon_{\text{s}}N}\left(V - V_{\text{bi}}\right), \tag{3.3}$$

where $C$ is the capacitance, $\varepsilon_0$ is the permittivity of free space ($8.854 \times 10^{-12}$ F m$^{-1}$), $A$ is the area of the capacitor ($\approx 10^{-6}$ m$^2$), $d$ is the thickness of the capacitor, $\varepsilon_{\text{s}}$ is the relative dielectric constant and $N$ is the charge carrier concentration of the material and $V_{\text{bi}}$ is the built-in potential in the heterojunction, where built-in potential is the voltage present at the interface of any two dissimilar materials due to their difference in work functions that results in a band bending.

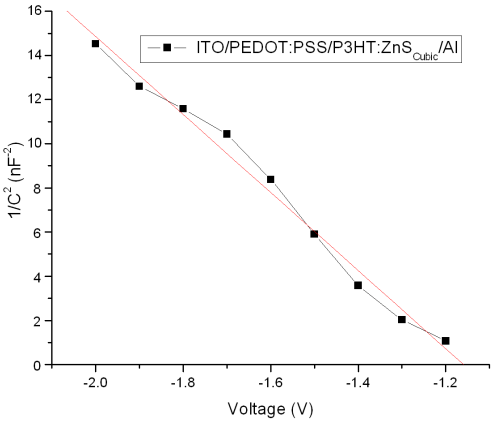


Fig. 5. $1/C^2$ vs. $V$ characteristics of ITO/PEDOT:PSS/P3HT:ZnS$_{\text{cubic}}$/Al (slope $= -1.767 \times 10^{19}$ F$^{-2}$ V$^{-1}$).

The experimental results shown in Figs. 5 and 6 follow Eq. (3.3) (the Mott–Schottky curve) which exhibits a straight line over a small bias voltage only and this reverse bias capacitance Mott–Schottky behaviour indicate the formation of a Schottky junction (band bending) at the P3HT:ZnS-Al contact.

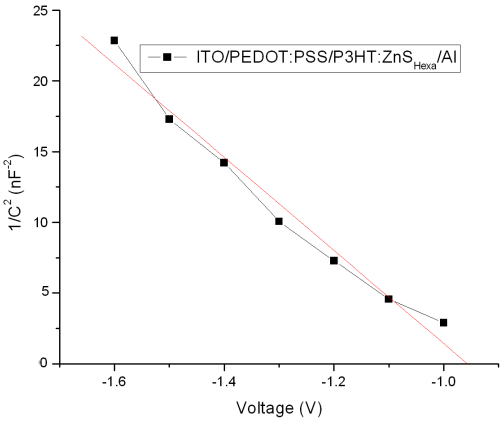


Fig. 6. $1/C^2$ vs. $V$ characteristics of ITO/PEDOT:PSS/P3HT:ZnS$_{hexa}$/Al (slope = $-3.293 \times 10^{18}$ F$^{-2}$ V$^{-1}$).

The negative slope of the curve found by Origin 7.5 software confirms the hole conductivity in the active material [24]. The intercept of the curve with the voltage axis gives $V_{bi}$ and the product $\varepsilon_s N$ can be found from the intercept with the capacitance axis or from the slope of the curve. In the case of ITO/PEDOT:PSS/P3HT:ZnS$_{cubic}$/Al device $V_{bi}$ was found as –1.16 V and in the case of ITO/PEDOT:PSS/P3HT:ZnS$_{hexa}$/Al device $V_{bi}$ was found as –0.957 V. The shifting of the flat band potential (in-built potential) to the negative side under illumination is already reported [24] and this negative flat band potential is the result of band unpinning by charging a surface state at the metal/organic contact, that the surface state acquires more charge under illumination. There is an accumulation of minority carriers (with respect to dark conditions), which produces an increase of the quasi-Fermi level and an additional charge in the surface state. An important requirement for such an additional charging is a slow kinetics of charge transfer through the surface state. The additional charge at the surface state produces an increase of voltage in the dipole layer, and a displacement of the apparent flat band potential.

It is found that the depletion width of the device ITO/PEDOT:PSS/P3HT:ZnS$_{cubic}$/Al according to Eq. (3.2) for a reverse bias voltage between –2 V and –1.2 V resulted to be varying between 249 nm and 201 nm which is compatible with the thickness of the active layer 247 nm and the charge carrier concentration of the active material varied from $1.088 \times 10^{22}$ m$^{-3}$ to $2.952 \times 10^{21}$ m$^{-3}$. Similarly, the depletion region of the device ITO/PEDOT:PSS/P3HT:ZnS$_{hexa}$/Al for a reverse bias voltage between –1.6 V and –1.0 V resulted to be varying between 264 nm and 192 nm compatible with the active layer thickness 275 nm and the charge carrier concentration of the active material varied from $2.086 \times 10^{22}$ m$^{-3}$ to $7.433 \times 10^{21}$ m$^{-3}$ in that region. The remarkable result is that the hole concentration of P3HT:ZnS system is comparable to the hole concentration of the previously reported P3HT:PCBM system of Bisquert et al. [24]. They report [24] hole concentration about $3.5 \times 10^{22}$ m$^{-3}$ for P3HT:PCBM system where $V_{bi}$ and $\varepsilon$ was 0.43 V, 3 respectively, while the device parameters were $V_{oc} = 0.39$ V, $I_{sc} = 8.7$ mA cm$^{-2}$ and FF = 42%. It is obvious that the $V_{oc}$ of P3H:ZnS is higher (1.3 V [6]) than P3HT:PCBM system, but $J_{sc}$ and FF is very much lower than P3HT:PCBM and it may be due to the higher hole concentration or defects as reported in the case of CdTe solar cells [25], a-Si:H/c-Si heterojunction solar cells [26] and in P3HT:PCBM [27]. Trukhanov et al. [27] proved that the doping or the defects in the P3HT system results in substantial increase in $V_{oc}$ and decrease in $J_{sc}$ and FF.

## 4. Conclusion

The Mott–Schottky analysis of the bulk heterojunction solar cells of sphalerite and wurtzite ZnS incorporated P3HT shows the formation of a Schottky junction and band unpinning at the P3HT:ZnS-Al interface and it also confirms the hole conductivity in the active material. The remarkable result is that the hole concentration of P3HT:ZnS system is comparable to the hole concentration of the P3HT:PCBM system.

## Acknowledgments

The author acknowledge the support given by Dr A. Anu Kaliani, Kongunadu Arts and Science College, Coimbatore, Dr. Arun D. Rao and Dr. Praveen C. Ramamurthy (Department of Materials Engineering), INUP and CEN @ IISc., Bangalore for completing this work.

## References

[1] A. Iwan, A. Chuchmała, *Prog. Polym. Sci.* **37**, 1805 (2012).

[2] M. Palewicz, A. Iwan, *Curr. Phys. Chem.* **1**, 27 (2011).

[3] Li-Min Chen, Ziruo Hong, Gang Li, Yang Yang, *Adv. Mater.* **21**, 1434 (2009).

[4] D. Venkataraman, Serkan Yurt, B. Harihara Venkataraman, Nagarjuna Gavvalapalli, *J. Phys. Chem. Lett.* **1**, 947 (2010).

[5] Jiun-Tai Chen, Chain-Shu Hsu, *Polym. Chem.* **2**, 2707 (2011).

[6] T. Abdul Kareem, A. Anu Kaliani, *J. Nano- Electron. Phys.* **7**, 02026 (2015).

[7] M. Bredol, K. Matras, A. Szatkowski, J. Sanetra, A.P. Schwa, *Sol. En. Mater. Sol. Cells* **93**, 662 (2009).

[8] M. Mall, P. Kumar, S. Chand, L. Kumar, *Chem. Phys. Lett.* **495**, 236 (2010).

[9] B.R. Saunders, M.L. Turner, *Adv. Coll. Interf. Sci.* **138**, 1 (2008).

[10] A. Kongkanand, K. Tvrdy, K. Takechi, M. Kuno, P.V. Kamat, *J. Am. Chem. Soc.* **130**, 4007 (2008).

[11] W. Martienssen, H. Warlimont, *Springer Handbook of Condensed Matter and Materials Data*, 1st ed., Springer, New York 2005.

[12] Y. Yang, S. Xue, S. Liu, J. Huang, J. Shen, *Appl. Phys. Lett.* **69**, 377 (1996).

[13] T. Abdul Kareem, A. Anu Kaliani, *J. Nanostruct. Chem.* **3**, 56 (2013).

[14] T. Abdul Kareem, A. Anu Kaliani, *J. Nanostruct. Chem.* **3**, 31 (2013).

[15] T. Sun, Z.L. Wang, Z.J. Shi, G.Z. Ran, W.J. Xu, Z.Y. Wang, Y.Z. Li, L. Dai, G.G. Qin, *Appl. Phys. Lett.* **96**, 133301 (2010).

[16] J. Deboisblanc, M.Sc. Thesis, Department of Physics and Astronomy, Pomona College, California 2010.

[17] K.N. Rao, *Indian J. Pure Appl. Phys.* **42**, 201 (2004).

[18] E.J. Guo, H. Guo, H. Lu, K. Jin, M. He, G. Yang, *Appl. Phys. Lett.* **98**, 011905 (2011).

[19] R.H. Friend, R.W. Gymer, A.B. Holmes, J.H. Burroughes, R.N. Marks, C. Taliani, D.D.C. Bradley, D.A.D. Santos, J.L. Breâdas, M. Loègdlund, W.R. Salaneck, *Nature* **397**, 121 (1999).

[20] L.M. Chen, Z. Xu, Z. Honga, Y. Yang, *J. Mater. Chem.* **20**, 2575 (2010).

[21] Z. Hu, T. Daeri, M.S. Bonner, A.J. Gesquiere, *J. Lumin.* **130**, 771 (2010).

[22] Y. Zhao, G. Yuan, P. Roche, M. Leclerc, *Polymer* **36**, 2211 (1995).

[23] T. Kirchartz, W. Gong, S.A. Hawks, T. Agostinelli, R.C.I. MacKenzie, Y. Yang, J. Nelson, *J. Phys. Chem. C* **116**, 7672 (2012).

[24] J. Bisquert, G. Garcia-Belmonte, A. Munar, M. Sessolo, A. Soriano, H.J. Bolink, *Chem. Phys. Lett.* **465**, 57 (2008).

[25] H. Zhao, Ph.D. Thesis, University of South Florida, 2007.

[26] P. Gang, W. Xiaojing, T. Pengju, Z. Wenli, Y. Jun, in: *Proc. ISES World Congress 2007 Solar Energy and Human Settlement*, Eds. D. Yogi Goswami, Yuwen Zhao, ISBN 978-3-540-75997-3, Springer-Verlag, Berlin Heidelberg 2009, p. 1159.

[27] V.A. Trukhanov, V.V. Bruevich, D.Y. Paraschuk, *Phys. Rev. B* **84**, 205318 (2011).